Temperature Analysis and Characteristics of Highly Strained InGaAs–GaAsP–GaAs ($\lambda > 1.17$ μm) Quantum-Well Lasers

Nelson Tansu, Ying-Lan Chang, Tetsuya Takeuchi, David P. Bour, *Fellow, IEEE*, Scott W. Corzine, Michael R. T. Tan, and Luke J. Mawst, *Senior Member, IEEE*

***Abstract*—Characteristic temperature coefficients of the threshold current (T_0) and the external differential quantum efficiency (T_1) are studied as simple functions of the temperature dependence of the physical parameters of the semiconductor lasers. Simple expressions of characteristics temperature coefficients of the threshold current (T_o) and the external differential quantum efficiency (T_1) are expressed as functions as physical parameters and their temperature dependencies. The parameters studied here include the threshold ($J_{\rm th}$) and transparency ($J_{\rm tr}$) current density, the carrier injection efficiency ($\eta_{\rm inj}$) and external (η_d) differential quantum efficiency, the internal loss (α_i), and the material gain parameter (g_o). The temperature analysis is performed on low-threshold current density ($\lambda = 1.17$–1.19 μm) InGaAs–GaAsP–GaAs quantum-well lasers, although it is applicable to lasers with other active-layer materials. Analytical expressions for T_0 and T_1 are shown to accurately predict the cavity length dependence of these parameters for the InGaAs active lasers.**

***Index Terms*—Diode lasers, epitaxial growth, long-wavelength lasers, quantum-well lasers, semiconductor growth, semiconductor lasers, strain, temperature analysis.**

I. Introduction

THE EXPLOSION in the Internet and data transmission has led to an increased demand for higher bandwidth in optical fiber communications. The demand for higher bandwidth and longer transmission distance has led the pursuit of the single-mode 1.3-μm edge-emitters- or vertical-cavity surface-emitting lasers (VCSELs)-based systems, operating at a modulation bandwidth of 10 Gb/s, for the metro application using single-mode fiber, which will allow data transmission up to a distance of 20–30 km [1].

In order to realize low-cost 1.3-μm-based optical communications systems, high-performance (i.e., low-temperature-sensitive) diode lasers (either in-plane or VCSELs) are needed. However, conventional InP-based long-wavelength diode lasers, at $\lambda = 1.3$ μm, are inherently highly temperature sensitive [3], due to strong Auger recombination, large carrier leakage from the active layer, and intervalence band absorption. Typical values for the conduction-band offset for 1.3-μm InGaAsP-active on InP-substrate lasers are 204 meV [2], resulting in severe carrier leakage out of the quantum wells (QWs) [3] as well as increased Auger-assisted carrier leakage [4]. These factors lead to a high sensitivity of the laser performance to temperature changes and, as a result, additional electronics are needed to maintain the operational temperature of the lasers. This additional temperature controller will lead to a significant increase in the laser packaging cost [3]. Contrary to InP-based lasers, very large conduction band offset (471 meV) [23] can be achieved for a 1.3-μm emitting QW active with GaAs confinement layers. The large band offset helps suppress carrier leakage out of the QW to the confining region [1] and also the Auger-assisted carrier leakage [4].

Another major factor motivating the development of 1.3-μm GaAs-based diode lasers is the ease in forming high-quality (Al)GaAs–AlAs distributed Bragg reflectors (DBRs) on GaAs substrates [5]. Although many attractive alternative approaches have also been proposed on InP, e.g., by wafer bonding [6], metamorphic DBRs [7], and Sb-based DBRs [8], results have been inferior to typical GaAs-based VCSELs.

An attractive approach for achieving long-wavelength laser emission on GaAs substrates is the use of highly strained InGaAs [9]–[13] or InGaAsN [1], [14]–[19] QWs. The use of highly strained InGaAs QW active lasers to extend the emission wavelength to 1.20 μm was pioneered by Sato *et al.* [10] and Iga and Koyama *et al.* [11], [12]. Recently, GaAsP tensile barriers have also been implemented to strain-compensate the InGaAs QW [9], [13]. Contrary to 1.3-μm lasers on InP, recent studies on recombination mechanisms in InGaAsN–GaAs lasers, at 1.3 μm, have shown that Auger recombination is not the dominant recombination processs in this material system [20].

We describe here optimization of highly strained InGaAs material optical quality and laser structure design which is expected to lead to significantly higher performance from MOCVD grown devices, including the compressively strained $In_{0.35}Ga_{0.65}As$ QW (laser A), a strain-compensated $In_{0.35}Ga_{0.65}As$–$GaAs_{0.85}P_{0.15}$ QW (laser B), and the strain-compensated $In_{0.4}Ga_{0.6}As$–$GaAs_{0.85}P_{0.15}$ QW (laser C). A comprehensive temperature analysis of the InGaAs QW devices is performed based on the temperature dependencies of the physical parameters, as discussed in Section V.

II. Design Considerations

The method of incorporating very low N content (<0.5%) in high In content InGaAs QWs was first proposed by Sato *et al.*

Manuscript received August 7, 2001; revised February 25, 2002.

N. Tansu and L. J. Mawst are with the Department of Electrical Computer Engineering, University of Wisconsin-Madison, Madison, WI 53706 USA (e-mail: tansu@cae.wisc.edu).

Y.-L. Chang, T. Takeuchi, D. P. Bour, S. W. Corzine, and M. R. T. Tan are with the Communications and Optics Research Labs, Agilent Technologies Laboratories, Palo Alto, CA 94304 USA.

Publisher Item Identifier S 0018-9197(02)05024-8.

[15]. The use of high In content (approximately 35%) allows an InGaAsN QW with low N content (about 0.5%) to reach emission wavelengths of 1.3 μm with improved optical luminescence over that of the high N content alloys.

Extending the emission wavelength of the InGaAs QW diode laser grown by MOCVD relies on two techniques. The first technique to extend the emission wavelength is by growing the InGaAs active region at a reduced temperature in the range 510 °C–550 °C. Previous studies have shown improvement in the optical luminescence of the materials grown at reduced temperature due to a reduction in dislocation density in the materials [9], [13], [21]. By growing the InGaAs QW at a reduced temperature, the surface energy during the growth is lowered compared to the energy to form dislocations, which will in turn increase the effective critical thickness of the materials [22], [23]. The temperature-dependent critical thickness has also been shown theoretically [22] and experimentally [23], with the lower substrate temperature resulting in larger critical thickness. Other techniques to calculate the critical thickness have also been proposed by Schlenker *et al.* [24]. Based on the model by Schlenker *et al.* [24], for an $In_{0.35}Ga_{0.65}As$ QW, the critical thickness is approximately 83 Å, which, as expected, is slightly higher than the critical thickness calculated with the People and Bean model (75 Å). For most of our InGaAs QW laser structures studied here, we employ an $In_xGa_{1-x}As$ QW ($x = 0.35$–0.4) with a thickness of 60–80 Å for the active region.

The second technique to both improve performance and extend the emission wavelength of the highly strained InGaAs QW laser is the implementation of strain compensation for the active region. The use of tensile-strained GaAsP barriers surrounding the InGaAs QW [9], [13] is beneficial in two ways. The first benefit is associated with strain compensation, that is, the total strain of the QW and the barriers surrounding the QW will be lowered due to the existence of the tensile barriers. The reduced total strain of the QW and the barriers may lead to an increase in the effective critical thickness of the InGaAs QW. The second benefit of employing GaAsP barriers is the higher bandgap provided by the GaAsP barrier around the InGaAs or InGaAsN QW, which leads to a reduced carrier leakage out of the QW, and possibly a reduction in the Auger-assisted carrier leakage [4]. As a result, stronger carrier confinement in the QW lowers the temperature sensitivity of both the threshold current density and also the external differential quantum efficiency of the diode laser [9]. In our experiments, tensile strain barriers of (−0.6%) $GaAs_{0.85}P_{0.15}$ and (−1.2%) $GaAs_{0.67}P_{0.33}$ have been implemented and studied in the InGaAs QW structures.

III. MOCVD Growth Studies

All the quantum well structures studied here were grown by low-pressure metalorganic chemical vapor deposition (LP-MOCVD) on nominally exact (100) n-GaAs substrates. The [AsH_3]/III ratio was in excess of 100 for the InGaAs-active laser structures, but was reduced ([AsH_3]/III = 10–20) for the incorporation of nitrogen in the InGaAsN structures. Trimethylgallium (TMGa), trimethylaluminum (TMAl), and trimethylindium (TMIn) are used as the group III sources. For the group V sources, AsH_3 (100%) and PH_3 (100%) are used. Dilute (2% in Hydrogen) SiH_4 and dielthylzinc (DEZn) are used for the n- and p-dopants, respectively. The basic separate confinement heterostructure (SCH) InGaAs-active structures is shown in Fig. 1. Implementation of GaAsP and InGaP strain-compensation layers into the structure will be discussed later. The characterization of the strain and composition of the QW were obtained by using high-resolution X-ray diffraction experiments (HR-XRD), secondary ion mass spectroscopy (SIMS) experiments, and photoluminescence studies. From the HR-XRD and SIMS experiments, the composition of the $In_xGa_{1-x}As$ can be determined to be approximately 33%–35% In, which corresponds to approximately 2.45% compressive strain. The thickness of the InGaAs QW, measured by TEM, is determined to be approximately 79 Å. The typical peak wavelength and full width at maximum (FWHM) of the measured room-temperature photoluminescence spectra for the $In_{0.35}Ga_{0.65}As$ QW is approximately 1.16–1.188 μm and 26–27 meV (Fig. 2).

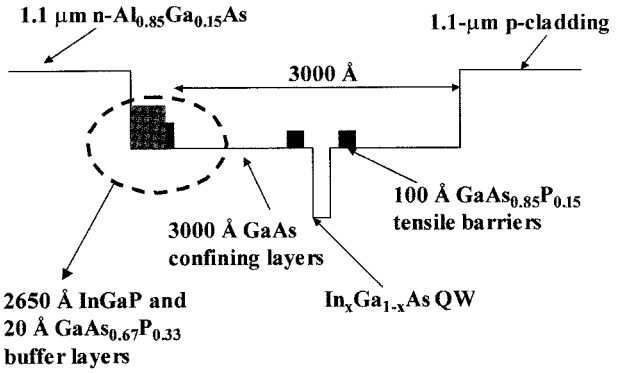

Fig. 1. Schematic energy bandgap diagram for the basic structure of the GaAsP strain-compensated highly strained $In_xGa_{1-x}As$ QW edge-emitting lasers.

By reducing the thickness of the QW to 60 Å and increasing the In content as high as 40%, the $In_{0.4}Ga_{0.6}As$ QW exhibits strong optical luminescence, as shown in Fig. 2. The peak photoluminescence wavelength for the $In_{0.4}Ga_{0.6}As$ QW is approximately 1.210 μm, with an FWHM of 29 meV. We observe a reduction of approximately 50% in the peak intensity of the photoluminescence of the $In_{0.4}Ga_{0.6}As$ QW, compared to that of the $In_{0.35}Ga_{0.65}As$ QW. Although the optical luminescence intensity for the 40% In content InGaAs is reduced, we find that the $In_{0.4}Ga_{0.6}AsN$ QW has stronger optical luminescence intensity compared for the $In_{0.35}Ga_{0.65}AsN$ QW, due to the reduced required nitrogen, to achieve 1.3-μm emission [19].

As shown in Fig. 1, n-$Al_{0.85}Ga_{0.15}As$ QW, grown at 800 °C, is used as the lower cladding layer, in order to represent the AlGaAs-based n : DBR in future VCSEL structures. Above the n-$Al_{0.85}Ga_{0.15}As$ cladding, a film of n-$In_{0.48}Ga_{0.52}P$, grown at 700 °C, enables us to explore the possibility of strain compensation through the use of tensile-strained InGaP below the compressively strained InGaAs(N) QW. The use of a 50-Å n-GaAs transitional layer, between the n-AlGaAs and the n-InGaP, is used to allow the temperature ramping (from 800 °C to 700 °C) to be performed with GaAs on the top surface.

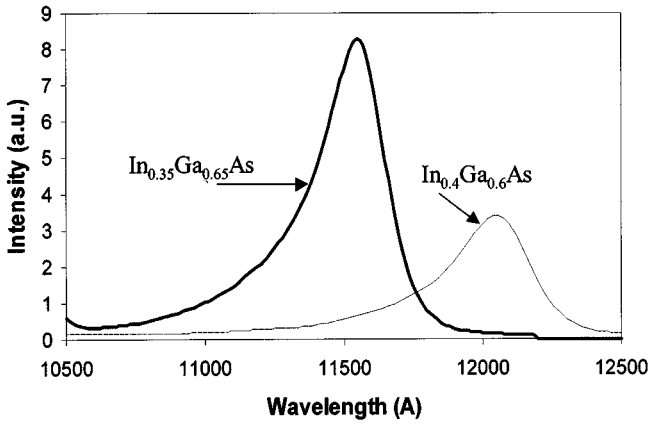

Fig. 2. Photoluminescence comparison between an 80-Å $In_{0.35}Ga_{0.65}As$ QW and a 60-Å $In_{0.4}Ga_{0.6}As$ QW.

The insertion of transitional layers of 20 Å of u-$GaAs_{0.67}P_{0.33}$ between the n-InGaP and the u-GaAs confining layers improves the InGaP–GaAs interface [25]. A transitional layer of 50 Å of u-GaAs is also used after the u-$GaAs_{0.67}P_{0.33}$ so the temperature ramping from 700 °C to 550 °C is performed with GaAs on the top surface. Both the GaAs confining regions and InGaAs QW are grown at a temperature of 550 °C. We find that the buffer layer of InGaP–GaAsP is essential for the growth of $In_{0.4}Ga_{0.6}As$ QWs on a high Al-content AlGaAs bottom cladding layer [19].

Our original structures (lasers A and B) utilize p-$In_{0.48}Ga_{0.52}P$, grown at 650 °C, for the top cladding layer, with three purposes. The first purpose is that the growth of InGaP materials for the top cladding will allow us the possibility of exploring etch and regrowth processes for the fabrication of index-guided device structures [26], [27], due to the low surface recombination velocity and low reactivity to O_2. The second purpose of the use of the InGaP for the p-cladding is for temperature control for the annealing of the InGaAsN QW in our future studies. Annealing of InGaAsN is commonly performed during the growth of the p-cladding [28]. By using InGaP as the material for the p-cladding, which can be grown with high optical quality in a wide range of temperature from 600 °C to 725 °C, larger flexibility in selecting the *optimal* growth temperature for the *in situ* anneal of the InGaAsN QW can be gained. By contrast, the growth of a high-quality p : AlGaAs based cladding layer generally employs a growth temperature above 750 °C. Finally, the series resistance of the Al-free materials also makes InGaP an attractive choice of material for the p-cladding [29].

Laser C (utilizing $In_{0.4}Ga_{0.6}As$ QW) utilizes modified cladding layers, with n- and p-cladding layers formed by 1.1-μm $Al_{0.74}Ga_{0.26}As$. The impact of changing from p-InGaP to p-AlGaAs for laser C is discussed in Section IV-B. Higher performance is achieved with the p-AlGaAs cladding layer, due to the elimination of carrier leakage through interfacial defects between the interface of the p-InGaP and udoped-GaAs confining region.

Material characterization of the active region was also performed, on the structure in Fig. 1, by employing high-resolution transmission electron microscopy (HR-TEM). The atomic level HR-TEM image of our $In_{0.35}Ga_{0.65}As$ QW appears to be compositionally more abrupt at the leading edge of the QW compared to the trailing edge [30]. From the image of HR-TEM studies on the highly strained $In_{0.35}Ga_{0.65}As$ QW, the existence of line dislocations in the $In_{0.4}Ga_{0.6}As$ QW is not observed.

IV. Broad-Area Laser Analysis: Highly Strained InGaAs QW-Active Lasers

A. Method and Theory of Laser Characterization

Several laser structures are fabricated and studied. Laser structures A and B utilize the highly strained 80-Å $In_{0.35}Ga_{0.65}As$ QW, without and with $GaAs_{0.85}P_{0.15}$ strain compensation, respectively. Laser C utilizes a higher In content $In_{0.4}Ga_{0.6}As$ QW, with $GaAs_{0.85}P_{0.15}$ strain compensation. The strain-compensated structure is shown in Fig. 1. The uncompensated structure is similar to the structures in Fig. 1, only without the GaAsP tensile barriers. As stated in the previous section, lasers A and B utilize n-$Al_{0.85}Ga_{0.15}As$ and p-InGaP as the cladding layers. By contrast, laser C uses n-$Al_{0.74}Ga_{0.26}As$ and p-$Al_{0.74}Ga_{0.26}As$ as the cladding layers. The GaAsP tensile barriers have previously been shown to improve the performance of highly strained InGaAs QW lasers near the 1.2-μm wavelength regime [9], [13]. The $GaAs_{0.85}P_{0.15}$ barriers, which are approximately 75 Å each, are grown approximately 100 Å before and after the InGaAs QW. Lasers with higher P-content GaAsP tensile barriers, and higher doping-level p-cladding layers for suppression of carrier leakage to the cladding [31], [32], are also studied in the device optimizations (Section IV-B).

All the semiconductor wafers are processed into 100-μm-wide broad-area lasers of various lengths, with stripes defined in the (001) direction by the vertical grooves etched to the top cladding layers. The etching of the cap layers of GaAs is accomplished using an $NH_4OH : H_2O_2 : H_2O$ (3 : 1 : 50) solution, which is selective to InGaP materials. An oxide-defined stripe geometry is then used to confine the current into the gain medium.

The above laser structures are characterized by extracting the device parameters from measurements on various cavity-length broad-area ($w = 100$ μm) diode lasers. The extracted device parameters include the threshold ($J_{\rm th}$) and transparency ($J_{\rm tr}$) current density, current injection efficiency ($\eta_{\rm inj}$), external differential quantum efficiency (η_d), temperature characteristic coefficients of threshold current density (T_0) and external differential quantum efficiency (T_1), internal loss (α_i), and material gain parameter (g_o). The optical confinement factor for the QW active region in all the laser structures is designed to be approximately 2.2%. All the length studies to extract the physical parameters of the lasers are performed on as-cleaved devices under low duty-cycle pulsed operation (6 μs, 1 kHz). We assume the reflectance value $R = 0.29$, for the as-cleaved facets. The errors in the analysis of the multi-length studies, in determining the above-threshold current injection efficiency ($\eta_{\rm inj}$) and the internal loss (α_i), are due to the uncertainty in determining the intercept from these length studies. The multi-length studies, which are commonly used [3], [44], [45], [47], assume the internal loss to be independent of carrier density. An alternative

measurement proposed by Andrekson *et al.* [57] allows more accurate measurement of internal loss; however, we chose to perform length studies here for simplicity.

In our analysis, the gain expression for QW lasers is assumed to follow the semi-logarithmic gain expression which is a function of material gain parameters (g_o), the fraction of injection current density in the QW ($\eta_{\rm inj}.J$), and the transparency current density in the QW ($J_{\rm tr}$) [33], [34]. This semi-logarithmic threshold-gain expression is

$$g_{\rm th} = g_o \cdot \ln(\eta_{\rm inj} \cdot J_{\rm th}/J_{\rm tr}). \quad (1)$$

Using the threshold condition $\Gamma g_{\rm th} = \alpha_i + (1/L)\ln(1/R)$, the threshold current density for a single QW laser can then be expressed as follows:

$$J_{\rm th} = \frac{J_{\rm tr}}{\eta_{\rm inj}} \cdot \exp\left(\frac{\alpha_i + (1/L)\ln(1/R)}{\Gamma g_o}\right) \quad (2)$$

where $\eta_{\rm inj}$ is the current injection efficiency (i.e., the fraction of current density entering the active region), which equals the internal quantum efficiency as measured above laser threshold. It is important to clarify that the η_{inj} of interest here is the current injection efficiency, which is distinct from the internal efficiency (η_i). The internal efficiency is a function of internal quantum efficiency (η_q), current injection efficiency ($\eta_{\rm inj}$) and the lateral-pumping efficiency ($\eta_{\rm lateral}$) [56]. The $\eta_{\rm lateral}$ for the broad area lasers, with a 100-μm-wide stripe, and the above threshold η_q is expected to be close to unity.

The use of $\eta_{\rm inj}$ in (2) enables us to determine the *internal* transparency current density $J_{\rm tr}$, which is a function of nonradiative (defect-induced), radiative, and Auger recombination in the QW. By taking into account only the fraction of threshold current density that contributes to recombination (including nonradiative, radiative, and Auger processes) within the QW ($\eta_{\rm inj} \cdot J_{\rm th}$), the *internal* transparency current density should be unchanged for structures with similar active regions, regardless of modifications to the device structure which may effect the carrier injection efficiency. Equation (2) can be rearranged as

$$\alpha_i + (1/L)\ln(1/R) = \Gamma g_o \ln(\eta_{\rm inj} \cdot J_{\rm th}) - \Gamma g_o \ln(J_{\rm tr}). \quad (3)$$

From the threshold condition expressed in (3), the threshold gain can be plotted against the logarithm of $\eta_{\rm inj} \cdot J$, and the slope of the resulting line will give us the $\Gamma \cdot g_o$ value. Also, the intercept of the plot of (3), with the x axis, will yield the transparency current density. The peak differential gain at transparency β_{tr} is defined as $\beta_{\rm tr} = dg/dJ$ ($J = J_{\rm tr}$), which can then be written as $\beta_{\rm tr} = g_o/J_{\rm tr}$. Differential gain values at transparency and also at threshold are important parameters in determining the maximum modulation frequency of the diode laser. Characterization of the characteristic temperature coefficients for the threshold current density and external differential quantum efficiency are performed over the temperature range of 20 °C–70 °C. In addition to the threshold current density and the external differential efficiency, the temperature characterization of the current injection efficiency, internal loss, transparency current density, and material gain parameters are investigated. The optical field profiles for all the laser structures studied here are designed to be similar with each other for consistency in the comparative experiments described below.

TABLE I
PERFORMANCE OF $In_{0.35}Ga_{0.65}As$ (SAMPLE A), $In_{0.35}Ga_{0.65}As$–$GaAs_{0.85}P_{0.15}$ (SAMPLE B), $In_{0.4}Ga_{0.6}As$–$GaAs_{0.85}P_{0.15}$ (SAMPLE C) DIODE LASERS FOR 100-μm-WIDE × 1-mm-LONG DEVICES

L=1000μm	Laser A	Laser B	Laser C
QW	$In_{0.35}Ga_{0.65}As$	$In_{0.35}Ga_{0.65}As$	$In_{0.4}Ga_{0.6}As$
Barriers	GaAs	$GaAs_{0.85}P_{0.15}$	$GaAs_{0.85}P_{0.15}$
t_{QW} (Å)	79	60	60
λ(μm)	1.170	1.170	1.185
J_{th} (A/cm²)	125	70	130
J_{tr} (A/cm²)	35	30	59
η_d (%)	29	50	53
η_{inj} (%)	37	60	79
α_i (cm^{-1})	5	2	6
g_o (cm^{-1})	1800	1975	1600
T_0 (K)	180	120	200
T_1 (K)	800	300	750

B. Laser Characteristics

All the extracted experimental data ($L = 1000$ μm) for samples A, B, and C are all presented in Table I. The low current injection efficiency, $\eta_{\rm inj}$, (∼37%) of laser A is the cause of the low external differential efficiency (∼29%–33%) of this device structure. The temperature characteristic coefficients of the threshold current density (T_0) and external differential quantum efficiency (primary T_1) for these lasers (A) are found to be anomalously high. These high values of T_0 and T_1 may be related to a high defect density, as described below.

By incorporating $GaAs_{0.85}P_{0.15}$ tensile barriers (sample B), significant improvement in the lasing performance of the InGaAs QW lasers is obtained. In sample B, threshold and transparency current density of as low as 65 A/cm^2 (for $L =$ 1500 μm) and 30 A/cm^2 are measured respectively. External differential quantum efficiencies as high as 56% are measured for shorter cavity laser diodes (for $L = 500$ μm). The measured room-temperature peak lasing wavelength for this particular lasers (sample B) is approximately 1.165 μm. The inclusion of the GaAsP barriers results in a significant improvement of the $\eta_{\rm inj}$ (61%) from laser B compared to that of laser A. The low $\eta_{\rm inj}$ (54%–60%) of the highly strained InGaAs QW lasers, at nearly 1.2 μm, with InGaP cladding layers has also been reported by Chen *et al.* [35] and Kondo *et al.* [36]. Possible causes for the observed low internal efficiencies are discussed in Section V.

The material gain parameter, g_o, and the transparency current density, $J_{\rm tr}$, are extracted, from (3) by fitting the measured threshold current density with various cavity lengths, to be approximately 1975 cm^{-1} and 30 A/cm^2, respectively. From the values of the g_o and $J_{\rm tr}$ derived above, the peak differential gain at transparency $\beta_{\rm tr}$ can be determined to be approximately 66 cm/A. The observed reduction in the characteristic temperature coefficients (T_0 and T_1) of laser B is presumably due to the reduction in dislocation density in the QW active region. Large

nonradiative recombination will lead to temperature-insensitive lasers.

In order to rule out the possibility that the large value of the strain of the InGaAs QW is a factor responsible for the low $\eta_{\rm inj}$, we reduce the strain in the QW (same thickness, $\Delta a/a = 1.5\%$) to achieve an emission wavelength of 1.06 μm. From this experiment, the extracted $\eta_{\rm inj}$ is found to be comparable to that of sample A. Therefore, we can rule out the large strain in the QW as the major factor leading to the observed low $\eta_{\rm inj}$.

The use of $GaAs_{0.67}P_{0.33}$ as tensile barriers surrounding the $In_{0.35}Ga_{0.65}As$ QW is found to not improve the lasing performance any further. The highly doped p-cladding material is used to suppress electron leakage from the confining region into the top cladding. The modification of the Fermi level in the highly doped p-cladding material results in a higher barrier, leading to less electron leakage from the confining region [31], [32], [37]. Although the highly doped p-cladding should help in suppressing the carrier leakage from the confining region into the top p-cladding region, the $\eta_{\rm inj}$ of the highly-doped p-cladding laser is still low ($\eta_{\rm inj} = 57\%$), which is comparable to that ($\eta_{\rm inj} = 61\%$) of sample B. A significant increase (from $\alpha_i = 2$ cm^{-1} to 12 cm^{-1}) in the internal loss of the highly-doped p-cladding laser is observed. The increase in the internal loss in the sample, with high-doped p-cladding, can be attributed to the large field-overlap with the highly doped p-cladding in the narrow waveguide SCH structure [38]. Since the suppression of carrier leakage does not improve the $\eta_{\rm inj}$ of the lasers, there must be an additional channel that leaks or traps out 30%–40% of the injected carriers. Since the quasi-Fermi levels for the carriers in the confinement region are not pinned, even above threshold, nonradiative recombination results in the loss of carriers that interact with interfacial defects between the undoped-GaAs confining region and p-InGaP top cladding layers [32].

In support of our presumption, recent improvement in $\eta_{\rm inj}$ from 54% to 89% by replacing the InGaP cladding layers with AlGaAs cladding layers has been demonstrated by Kondo *et al.* [36]. The improved interface between GaAs and AlGaAs, compared to GaAs–InGaP, reduces the nonradiative recombination due to a reduction in the interfacial defect density of the GaAs–AlGaAs interface. The temperature analysis, presented in Section V, also identifies carrier loss through interfacial defects, between p-InGaP and u-GaAs, as a possible leakage channel.

By replacing the p-InGaP with p-$Al_{0.74}Ga_{0.26}As$ for the top cladding of laser C, significant improvement in the $\eta_{\rm inj}$ of laser C, $\eta_{\rm inj} = 80\%$, is observed. The threshold- and transparency-current densities of laser C that utilizes a strain-compensated 60-Å $In_{0.4}Ga_{0.6}As$ QW are 100 A/cm^2 (for $L = 1500$ μm) and 59 A/cm^2, respectively. These $J_{\rm th}$ and $J_{\rm tr}$ of laser C are slightly higher than those of strain-compensated $In_{0.35}Ga_{0.65}As$ QW lasers (B). This increase in $J_{\rm tr}$ and $J_{\rm th}$, in laser C is expected due to the lower optical luminescence of the $In_{0.4}Ga_{0.6}As$ QW as compared to that of the $In_{0.4}Ga_{0.6}As$ QW. Even though the lasing performance of $In_{0.4}Ga_{0.6}As$ QW is poorer compared to that of $In_{0.35}Ga_{0.65}As$ QW, the optical luminescence of the $In_{0.4}Ga_{0.6}AsN$ QW is stronger than that of $In_{0.35}Ga_{0.65}AsN$ QW due to the lower required N, for the $In_{0.4}Ga_{0.6}AsN$ QW, to achieve 1.3-μm emission [19].

V. Temperature Analysis of the InGaAs QW Lasers

A. Temperature Analysis of the Threshold Current and Differential Quantum Efficiency

The primary motivation for the temperature analysis presented here is to express the T_0 and T_1 values in simple and more intuitive expressions, for the purpose of analyzing the temperature sensitivity of semiconductor lasers. The T_0 and T_1 values are expressed as functions of the physical parameters and their temperature dependencies. The simple forms of the T_0 and T_1 expressions should allow for practical identification and insight in determining the dominant mechanisms controlling the temperature sensitivity of diode lasers. The laser performance and extracted physical parameters are studied as a function of temperature, within the temperature range 20 °C–70 °C for samples B ($In_{0.35}Ga_{0.65}As$ QW) and C ($In_{0.4}Ga_{0.6}As$ QW). The parameters studied here include the threshold ($J_{\rm th}$) and transparency ($J_{\rm tr}$) current density, the current injection ($\eta_{\rm inj}$) and external differential (η_d) efficiency, internal loss (α_i), and material gain parameter (g_o).

The measurements of the variation of the threshold current density and the external differential quantum efficiency with temperature changes over 20 °C–70 °C are conducted on broad-area lasers, with a stripe width of 100 μm and various cavity lengths (L = 500–2000 μm). From the measured threshold current density and the external differential quantum efficiency for each cavity length at various temperatures, temperature-dependent internal device parameters are extracted. For each temperature, the inverse of the current injection efficiency ($\eta_{\rm inj}$) can be extracted from the intercept of the plot of the inverse of the external differential quantum efficiency ($1/\eta_d$) as a function of cavity length (L) with the $1/\eta_d$ axis. The internal loss α_i, for each temperature, can be extracted from the slope of the plot of the inverse of the external differential quantum efficiency ($1/\eta_d$) as a function of the cavity length (L). Once the internal loss and internal efficiency for various temperatures have been extracted, the modal material gain parameter ($\Gamma.g_o$), at each temperature can be extracted from the slope of the plot of the threshold modal gain ($\Gamma \cdot g_{\rm th}$) as a function of logarithm of the internal threshold current density [$\ln(\eta_{\rm inj} \cdot J_{\rm th})$] for each temperature, using (3). The intersect of the semi-logarithmic linear regression of $\Gamma \cdot g_{\rm th}$ versus $\ln(\eta_{\rm inj} \cdot J_{\rm th})$ with the $\ln(\eta_{\rm inj} \cdot J_{\rm th})$ axis will allow us to extract the transparency current density ($J_{\rm tr}$). All these processes are reiterated for each temperature from 20 °C to 70 °C with a temperature step of 5 °C. After reiterating the process over the entire temperature range, the characteristic temperature coefficients of the threshold and transparency current density, the internal and external differential quantum efficiency, the internal loss, the gain parameters, and the transparency current density are extracted.

The temperature dependence of the threshold current density (T_0) and the external differential quantum efficiency (T_1) empirically follow the known equations

$$J_{\rm th}(T) = J_{\rm tho} \cdot e^{(T/To)} \tag{4}$$

$$\eta_d(T) = \eta_{do} \cdot e^{-(T/T1)}. \tag{5}$$

To understand the different contributions to the characteristic temperature coefficient of the threshold current density (T_0), it is informative to express it in a different form. The threshold current density $J_{\rm th}$ can be expressed as shown in (2) and the modal threshold gain can be expressed as a function of internal loss and mirror loss: $\Gamma \cdot g_{\rm th} = \alpha_i + (1/L)\ln(1/R)$. By taking the derivative of $J_{\rm th}$ in (2) with respect to temperature changes, while assuming all the physical parameters to be temperature-dependent, we can write $dJ_{\rm th}/dT$ as follows:

$$\frac{dJ_{\rm th}}{dT} = \frac{1}{J_{\rm tr}} \cdot \frac{dJ_{\rm tr}}{dT} \cdot J_{\rm th} - \frac{1}{\eta_{\rm inj}} \cdot \frac{d\eta_{\rm inj}}{dT} \cdot J_{\rm th} + J_{\rm th} \cdot \frac{g_{\rm th}}{g_o} \cdot \left(\frac{1}{g_{\rm th}} \cdot \frac{dg_{\rm th}}{dT} - \frac{1}{g_o} \cdot \frac{dg_o}{dT} \right). \quad (6)$$

The internal efficiency (η_i), extracted from the multi-length studies, is essentially the above-threshold current injection efficiency ($\eta_{\rm inj}$). The above- and below-threshold current injection efficiencies are in general distinct from one another. A fundamental assumption of this analysis is that the above- and below-threshold current injection efficiency ($\eta_{\rm inj}$) and their temperature dependence ($T_{\eta{\rm inj}}$) are similar, which we expect to be reasonably accurate for comparing the temperature-behavior of the carrier loss processes in QW lasers with similar structures [58]. As long as carrier recombination within the SCH region does not increase rapidly above threshold, which can be confirmed from the linearity of the L–I curve, this assumption is expected to be accurate. The validation of this assumption is confirmed by experimental verification, in which the T_0 and T_1 expressions are shown to be accurate representations for devices with both large and reduced recombination in SCH. By assuming the transparency current density ($J_{\rm tr}$), internal efficiency (η_i), material gain parameter (g_o), and modal threshold gain ($\Gamma \cdot g_{\rm th}$) also vary exponentially with temperature (note that this assumption is validated by the experimental data shown in Figs. 3 and 4), we have

$$\frac{1}{T_{\rm tr}} = \frac{1}{J_{\rm tr}} \cdot \frac{dJ_{\rm tr}}{dT} \quad (7)$$

$$\frac{1}{T_{\eta_{\rm inj}}} = -\frac{1}{\eta_{\rm inj}} \cdot \frac{d\eta_{\rm inj}}{dT} \quad (8)$$

$$\frac{1}{T_{g_o}} = -\frac{1}{g_o} \cdot \frac{dg_o}{dT} \quad (9)$$

$$\frac{1}{T_{\alpha i}} = \frac{1}{\alpha_i} \cdot \frac{d\alpha_i}{dT}. \quad (10)$$

The only temperature-dependent term in the modal threshold gain ($T_{g{\rm th}} = g_{th}/(dg_{\rm th}/dT)$) is assumed to be that of the internal loss, since the mirror loss is assumed to be constant with temperature changes. The term $1/T_{g{\rm th}}(L)$ can also be expressed as $(1/T_{\alpha i}) \cdot \alpha_i/(\alpha_i + \alpha_m(L))$, with $1/T_{\alpha i} = (d\alpha_i/dT)/\alpha_i$.

From the relationship of the threshold current density with temperature changes in (4) and (6), we can reexpress the inverse of the characteristic temperature coefficient as follows:

$$\frac{1}{T_o(L)} = \frac{1}{T_{\rm tr}} + \frac{1}{T_{\eta_{\rm inj}}} + \frac{\alpha_i + \alpha_m(L)}{\Gamma \cdot g_o} \cdot \frac{1}{Tg_o} + \frac{\alpha_i}{\Gamma \cdot g_o} \cdot \frac{1}{T_{\alpha i}}. \quad (11)$$

A similar expression relating the T_0 values to the internal parameters has also been proposed by DeTemple and Herzinger [33]. From (11), the cavity length-dependent (L) terms in the T_0 formulation come in the modal threshold gain ($\Gamma \cdot g_{\rm th}(L)$) and the T_{go} terms. Just by using (12), we can observe that the T_0 values for shorter cavity devices are lower due to the higher modal threshold gain ($\Gamma \cdot g_{\rm th}$) in shorter cavity devices compared to those in longer cavity devices. As shown in Fig. 3, the theoretically calculated T_0 values, based on (11), agree well with the experimentally measured T_0 values. The structures shown are both for the optimized ($In_{0.4}Ga_{0.6}As$ QW—laser C) and unoptimized ($In_{0.35}Ga_{0.65}As$ QW—laser B) structures with emission wavelengths of 1.17–1.2 μm, in which the optimized structure exhibits strong suppression of recombination within the SCH. The un-optimized structure has a large defect-induced recombination in the interface between the cladding and the confinement region. Although the recombination in SCH is increased for the unoptimized structure, the calculated and measured T_0 values also compare very well with each other, with an error less than 5%. Further verification of the analysis presented has been performed on optimized InGaAs QW (λ = 980-nm) lasers, with strong carrier confinement in the QW's, also demonstrating errors of less than 5%. Several computational [39], [40], analytical [33], [41], and experimental [42], [43] results have also demonstrated similar behavior of an increase in the T_o value for longer cavity devices, in agreement with (11).

In order to characterize the temperature dependence of the external differential efficiency, one can go back to the fundamental

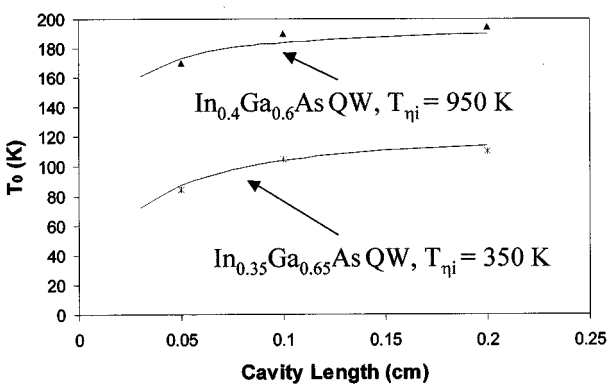

Fig. 3. T_0 values of structures of 1.2-μm lasers for laser B ($In_{0.35}Ga_{0.65}As$ QW) and laser C ($In_{0.4}Ga_{0.6}As$ QW), as functions of cavity length. The theoretical calculated values are shown by the solid line.

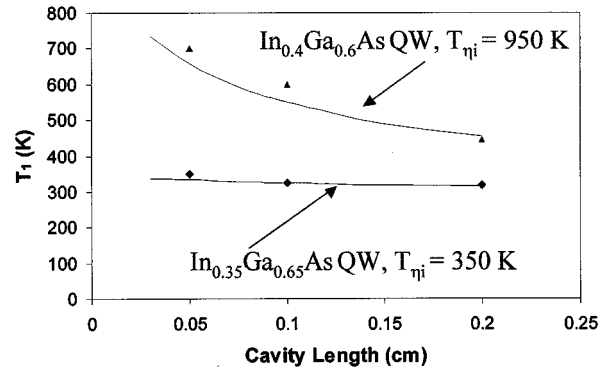

Fig. 4. T_1 values of structures of 1.2-μm lasers for laser B ($In_{0.35}Ga_{0.65}As$ QW) and laser C ($In_{0.4}Ga_{0.6}As$ QW), as functions of cavity length. The theoretical calculated values are shown by the solid line.

equation to express the external differential efficiency as a function of current injection efficiency, mirror, and internal loss as follows:

$$\eta_d = \eta_{\rm inj} \cdot \frac{\alpha_m(L)}{\alpha_i + \alpha_m(L)}. \tag{12}$$

As shown in (5), the temperature dependence of the external differential efficiency (T_1) can be expressed as a derivative of the external differential efficiency with respect to temperature. By taking into account the temperature dependence of the current injection efficiency and the internal loss, we can express the inverse of the T_1 value as follows:

$$\frac{1}{T_1(L)} = \frac{1}{T_{\eta_{inj}}} + \frac{\alpha_i}{\alpha_i + \alpha_m(L)} \cdot \frac{1}{T_{\alpha i}}. \tag{13}$$

In (13), the cavity-length-dependent term of the T_1 expression came from the modal threshold gain ($\Gamma \cdot g_{th}$) and the temperature dependence of the internal loss ($T_{\alpha i}$). As discussed above, the $\Gamma \cdot g_{\rm th}$ term increases as the cavity length decreases, which leads to a decrease in the T_1 values for the longer cavity, as shown in Fig. 4. The reduction in the T_1 value for longer cavity devices has also been observed experimentally in the 980-nm emitting InGaAs-active QW lasers [55]. The cavity length dependence of the T_1 values will be stronger for diode lasers with a low temperature sensitivity of the current injection efficiency (i.e., strong carrier confinement), which corresponds to very high $T_{\eta inj}$ values. As shown in Fig. 4, the T_1 values are expressed as a function of cavity length, for both laser C ($In_{0.4}Ga_{0.6}As$) and laser B ($In_{0.35}Ga_{0.65}As$) devices at $\lambda = 1.17$–1.2 μm. The theoretically predicted T_1 values are shown to accurately represent the experimentally observed trend of decreasing T_1 values with increasing cavity length [55]. The relationships between the $T_{\eta \rm inj}$ and $T_{\alpha i}$ will determine how significant is the dependence of the T_1 values on the cavity length.

B. Temperature Analysis of the Transparency Current Density

By analyzing the temperature behavior of the physical parameters in the T_0 and T_1 expressions in (11) and (13), further physical insight can be achieved by identifying the dominant controlling mechanisms of the T_0 and T_1 values. By identifying the mechanisms that lead to poor temperature characteristics of any given diode lasers, further improvement or changes in the device design can be pursued. In this analysis, the temperature dependencies of the transparency current density ($T_{\rm tr}$), current injection efficiency ($T_{\eta \rm inj}$), internal loss ($T_{\alpha i}$), and the material gain parameters (T_{go}) will be analyzed.

In order to further understand the characteristic temperature coefficient of the transparency carrier density ($T_{\rm tr}$), some additional analysis is needed. The transparency current density $J_{\rm tr}$ can be expressed as a function of the various recombination mechanisms as follows:

$$J_{\rm tr} = (A \cdot n_{\rm tr} + B \cdot n_{tr}^2 + C \cdot n_{\rm tr}^3) \cdot q.L_z \tag{14}$$

where A, B, C, and $n_{\rm tr}$ in (14) are the monomolecular, radiative, and Auger recombination coefficients and the transparency carrier density, respectively.

In the analysis, all pf the recombination coefficients A, B, and C, as well as the transparency carrier density ($n_{\rm tr}$), are all considered to be functions of temperature. The $dn_{\rm tr}/dT$ term is a positive value function, since the transparency carrier density of any given material will increase with increasing temperature due to the *smearing* of the Fermi–Dirac distribution function as the temperature increases [44], [45], [47]. Experimentally, the transparency carrier density has also been shown to have a strong dependence on temperature changes, in InP-based lasers, by Zou *et al.* [46]. To illustrate the dependence of $n_{\rm tr}$ quantitatively, one can express the simplified peak gain, g_p, as a function of the quasi-Fermi levels [47], with the assumption of zero scattering linewidth and only one occupied conduction and valence subband, as follows:

$$g_p(E) = g_m \cdot \lfloor f_c(E = E_{h1}^{e1}) - f_v(E = E_{h1}^{e1}) \rfloor. \tag{15}$$

The E_{h1}^{e1} term in (15) is defined as the energy level separation between the first conduction and the first valence subbands in the QW active region. The g_m value represents the gain coefficient determined by the transition matrix element and the 2-D reduced density of states. For an undoped QW active region, the electron carrier density (n) is assumed to equal the hole carrier density (p). Taking the approximation used by Vahala *et al.* [48], the quasi-Fermi level of the conduction band (f_c) and the valence band (f_v) can be approximated as

$$f_c(E = E_{h1}^{e1}) \cong 1 - e^{-n/nc} \tag{16a}$$

$$f_v(E = E_{h1}^{e1}) \cong e^{-p/nv} \tag{16b}$$

and the effective density of states for the conduction and valence band can be expressed as [47]

$$n_c \cong \frac{m_e^* \cdot k \cdot T \cdot \pi}{h^2 L_z} \sum_{n=1}^{\infty} e^{(E_{e1} - E_{en})/(kT)} \tag{17a}$$

$$n_v \cong \frac{m_h^* \cdot k \cdot T \cdot \pi}{h^2 L_z} \sum_{n=1}^{\infty} e^{(E_{hn} - E_{h1})/(kT)}. \tag{17b}$$

For the case of an undoped QW (with the condition $n = p$), the peak gain [see (15)] can then be expressed as a function of the carrier density n as follows:

$$g_p = g_m \cdot (1 - e^{-n/n_c} - e^{-n/n_v}). \tag{18}$$

The transparency carrier density is defined as the carrier density at which the peak gain g_p is equal to zero. The condition $g_p = 0$ occurs when $e^{-n/n_c} + e^{-n/n_v} = 1$. The transparency current density and its temperature dependence, based on (18) for various ratios of m_h/m_e, are shown in Fig. 5. From Fig. 5, it is clear that the transparency carrier density of the laser is approximately linearly proportional to the temperature. By taking the derivative of the transparency carrier density with respect to temperature, and dividing the result by the transparency carrier density ($n_{\rm tr}$), the values of $(1/n_{tr})dn_{tr}/dT$ (i.e., $1/T_{\rm ntr}$) can be extracted. The temperature dependence of $(1/n_{\rm tr})dn_{\rm tr}/dT$, also shown in Fig. 5, is found to be proportional to the inverse of the temperature T, independent of the ratio of the m_h/m_e ratio. From the argument given here, the value of $(1/n_{\rm tr})dn_{\rm tr}/dT$ (or $1/T_{\rm ntr}$) can be approximated with a high degree of accuracy by $1/T$, where T is the temperature of the measurement.

Both the nonradiative (A) and the radiative (B) recombination coefficients have a weak dependence on temperature changes [46]. Unlike the A and B coefficients, the Auger

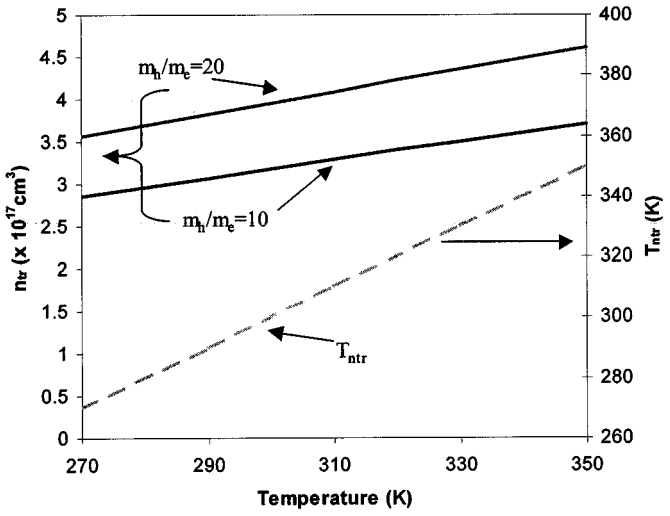

Fig. 5. The transparency carrier density ($n_{\rm tr}$) and its temperature characteristics ($T_{n{\rm tr}}$) as functions of temperature for $m_h/m_e = 10$ and 20.

recombination coefficient (C) is a strong function of temperature, especially in InP-based lasers [46], [3], [49]. For a limited temperature range, the A coefficient can be approximated as constant, since the A coefficient depends mostly on the dislocation density, in QWs and the SCH, that are constant over a limited temperature range. If the A coefficient is assumed to be a weak function of temperature, then dA/dT can be neglected. In laser structures for which the nonradiative recombination term is dominant, $T_{\rm tr}$ can then be approximated asymptotically as

$$T_{\rm tr}(A \gg B \cdot n_{\rm tr},\, C \cdot n_{\rm tr}^2) = n_{\rm tr} \cdot \frac{1}{\frac{dn_{\rm tr}}{dT}} = T. \qquad (19)$$

As expressed in (19), the $T_{\rm tr}$ values, at room temperature ($T \sim$ 300–350 K), for the case at which the nonradiative recombination term, is dominant will be close to 300–350 K.

There have been studies [50] where the temperature dependence of the bimolecular recombination coefficient, the B coefficient, is neglected. By contrast, there have also been several predictions [3], [51] that the expression for the B coefficient should be proportional to the inverse of the temperature, $1/T$. For our purposes, the model of the B coefficients can be expressed as $1/B \sim T^{1-x}$, in which x varies from 0 to 1. For the value of $x = 0$, this represents the model at which $B \sim 1/T$. For the case at which B is a weakly temperature-dependent function, the values of x will approach 1. By utilizing the expressions $(1/n_{\rm tr})dn_{\rm tr}/dT = 1/T$ and $1/B \sim T^{1-x}$, $T_{\rm tr}$ can also be approximated asymptotically, for the case in which the radiative recombination term is dominant, as

$$T_{\rm tr}(B \cdot n_{\rm tr} \gg A,\, C \cdot n_{\rm tr}^2) = \frac{T}{1+x}. \qquad (20)$$

By looking at (20), for measurements taken at room temperature ($T \sim$ 300 K), then the $T_{\rm tr}$ values, for the case in which radiative recombination is dominant, will be ranging from 150 K to 300 K depending on the dependence (x values) of the B coefficient on temperature changes. The values of $T_{\rm tr}$ for the case of radiative recombination dominated lasers at 980 nm is measured to be approximately 141 K [52], which falls into the range of the theoretically predicted $T_{\rm tr}$ values in (20).

For the case in which Auger recombination is dominant, we need to take into account the contribution of dC/dT. From [3] and [49], it has been shown that the Auger recombination coefficient can be approximated as $C = C_o \exp(-E_a/kT)$, where C_o is a temperature-independent coefficient and E_a is the activation energy for the Auger recombination process. Thus, the Auger recombination coefficient (dC/dT) can be approximated as $C_o \cdot (E_a/kT^2)\exp(-E_a/kT)$, which is *always* a *positive* function with a value decreasing toward zero as $T \to \infty$. By taking into account that the Auger recombination coefficient can be approximated as an exponential function of the activation energy and temperature, $T_{\rm tr}$ for the case in which the Auger recombination is dominant can be expressed as

$$T_{\rm tr}(C \cdot n_{tr}^2 \gg A,\, B \cdot n_{\rm tr}) = \frac{T}{\left(3 + \frac{Ea}{kT}\right)}. \qquad (21)$$

The quantity $\{E_a/(kT^2)\} \cdot n_{\rm tr} \cdot \{1/(dn_{\rm tr}/dT)\}$ always has a positive value and is a decreasing function with increasing temperature T. For the case of a laser with dC/dT approximately to zero, the predicted $T_{\rm tr}$ values are approximately less than three times smaller than the $T_{\rm tr}$ values for the nonradiative recombination dominated lasers. The activation energy E_a has been shown to range from 20 to 60 meV depending on the type of the active regions and the barriers surrounding the active regions [3], [51]. By assuming a room-temperature measurement ($T = 300$ K), and the activation energy, E_a, to range from 20 to 60 meV, the *predicted* $T_{\rm tr}$ values for the Auger recombination dominated lasers should range from 55 to 79 K, which is also in agreement with the *measured* $T_{\rm tr}$ (64 K) of InP-based 1.3-μm lasers [52].

From (19), we can now understand that the anomalously high values of T_0 are possibly a result of a strong nonradiative component in the transparency current. A high defect density results in a strong nonradiative recombination term in the characteristic temperature coefficient for the transparency current density. By contrast, the values of $T_{\rm tr}$ for Auger-recombination dominated lasers, such as InP-based 1.3–1.55 μm-emitting lasers, can be less (for the case $dC/dT \to$ zero) than one-third the values for the nonradiative recombination dominated lasers. The typical $T_{\rm tr}$ values for InGaAs QW on GaAs at 980 nm and InGaAsP QW on InP at 1.3 μm, are 141 K and 66 K, respectively [52]. As expected from (20), the value of $T_{\rm tr}$ for an InGaAs QW laser structure emitting at $\lambda = 980$ nm [52], which does not suffer from Auger recombination or major nonradiative recombination, has a much higher $T_{\rm tr}$ compared to InP-based lasers at 1.3 μm.

From this simple model of the temperature dependence of the transparency current density ($T_{\rm tr}$), one can determine whether Auger recombination is a major recombination mechanism in the active region of the semiconductor laser. For the lasers that suffer only minimal Auger recombination, the $T_{\rm tr}$ value should have values in the range of 150–350 K for measurements near room temperature, regardless of whether nonradiative or radiative mechanisms dominates the recombination. Only if the Auger recombination mechanism dominates will the values of $T_{\rm tr}$ be less than 80 K, as shown in Fig. 6.

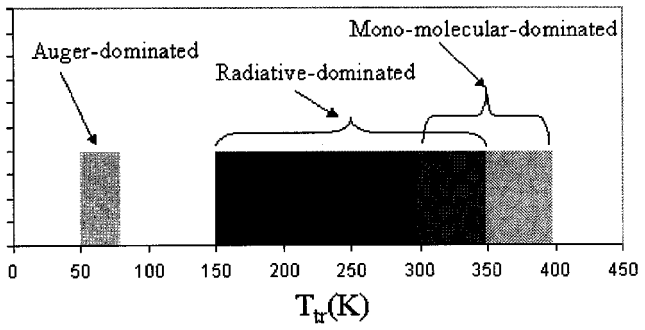

Fig. 6. The different regime of the $T_{\rm tr}$ values corresponding to different dominant recombination mechanisms. For the Auger dominated case, the $T_{\rm tr}$ value ranges from 50–80 K, which is very distinct from the radiative and nonradiative dominated case.

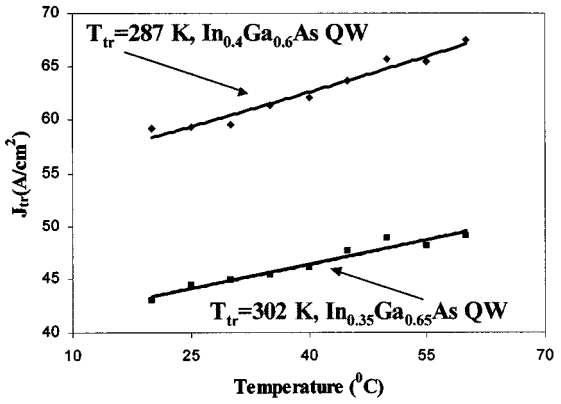

Fig. 7. The transparency current density $J_{\rm tr}$ as a function of temperature for $In_{0.35}Ga_{0.65}As$–$GaAs_{0.85}P_{0.15}$ QW active (sample B), and for $In_{0.4}Ga_{0.6}As$–$GaAs_{0.85}P_{0.15}$ QW active (sample C).

The transparency current density of the InGaAs QW ($\lambda = 1.17$–1.2 μm) lasers are analyzed as functions of temperature, as shown in Fig. 7 for lasers B ($In_{0.35}Ga_{0.65}As$) and C ($In_{0.4}Ga_{0.6}As$). The temperature dependences of both InGaAs QW structures are found to be similar, with $T_{\rm tr}$ values of 287–300 K. This high T_{tr} value, indicates that Auger recombination is not the dominant recombination processes, as expected at $\lambda = 1.2$ μm. These $T_{\rm tr}$ values may indicate there exists large monomolecular processes in the QW, presumably due to the use of the high strain values of the QW. The higher transparency current density of the $In_{0.4}Ga_{0.6}As$ QW devices, compared to that of the $In_{0.35}Ga_{0.65}As$ QW, may reflect higher defect density in the $In_{0.4}Ga_{0.6}As$ QW. The $T_{\rm tr}$ values, for sample A, are found to be as high as 360–400 K, which are attributed to the large monomolecular recombinations in the SCH, enhanced by the low $\eta_{\rm inj}$ in laser A.

The same temperature analysis of the transparency current density can be carried out in InGaAsN QW [60] or InP-based lasers to determine the role of Auger recombination in these laser structures. It is crucial to note that the temperature dependence of the threshold current density (T_0) is not solely a function of the recombination mechanisms reflected in the transparency current density. As shown in (12), the T_0 values can be affected by several factors: the recombination mechanism in the QW ($T_{\rm tr}$), carrier leakage ($T_{\eta \rm inj}$), intervalence band absorption (which effects $T_{g\rm th}$), and the temperature dependence of the material gain parameter (T_{go}). The suppression of Auger recombination within the QW active will improve the $T_{\rm tr}$ value, however, the T_o value may still be affected by the other mechanisms described above.

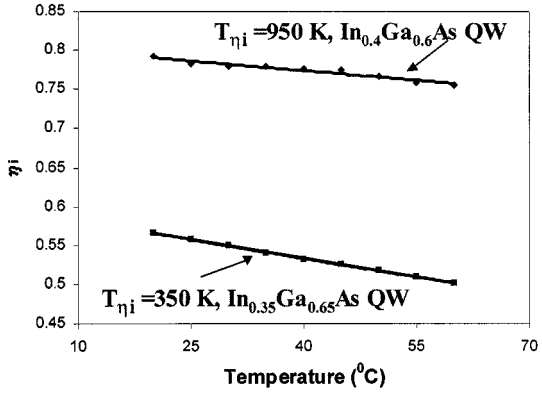

Fig. 8. The measured current injection efficiency η_i as a function of temperature for $In_{0.35}Ga_{0.65}As$–$GaAs_{0.85}P_{0.15}$ QW active (sample B), and for $In_{0.4}Ga_{0.6}As$–$GaAs_{0.85}P_{0.15}$ QW active (sample C).

C. Current Injection Efficiency, Internal Loss, and Material Gain Parameters

The temperature dependence of the current injection efficiency ($T_{\eta \rm inj}$) is an important parameter for characterizing carrier leakage from the InGaAs QW. Carrier leakage occurs through three kinds of mechanisms. The first mechanism is carrier leakage out of the QW into the confining region. The second mechanism is carrier leakage out of the confining region into the cladding region. The third mechanism is the "leakage" or loss of carriers through recombination in the SCH region, since the quasi-Fermi levels outside the QW are not pinned above the laser threshold [32]. If interfacial defects exist at the interface between the confining regions and the cladding regions, the carrier leakage path may occur through the carrier sinks created by the interfacial defects. A low value of $T_{\eta \rm inj}$ will indicate severe carrier leakage occurs through one of three mechanisms. The typical values of $T_{\eta \rm inj}$ for GaInAlAs QW lasers on InP at 1.55 μm and for InGaAsP QW lasers on InP at 1.3 μm are 106 K [53] and 64 K, [52] respectively. By contrast, for InGaAs QW lasers on GaAs substrates emitting at 980 nm, the values of $T_{\eta i}$ (in the 20 °C–60 °C range) can be extremely high [54]. Further studies are still required to understand further the controlling mechanisms in achieving a high $T_{\eta inj}$ design.

The temperature analysis of the current injection efficiency is carried out on the experiments involving InGaAs QW devices (lasers B and C), as shown in Fig. 8. In InGaAs QW lasers, the thermionic emission of the QW-confining and confining-cladding is expected to be minimal due to the large band-offset of the structures. The laser B structure has larger recombination in the SCH, due to the increase in the recombination due to the interfacial-defect in the confining-cladding interface, thereby resulting in a lower $T_{\eta \rm inj}$ of 350 K. By replacing the top cladding from p-InGaP to p-AlGaAs, the improved interface has resulted in a significant increase in the $T_{\eta \rm inj}$ up to 950 K from 350 K, evidenced in laser C. The high $T_{\eta \rm inj}$ values in laser C are

significant because they demonstrate that the use of a p-AlGaAs top cladding layer in laser C helps in suppressing the carrier loss mechanism as compared to that of laser B, and are reflected in the improved $\eta_{\rm inj}$ and $T_{\eta{\rm inj}}$ of laser C.

The temperature behavior of the internal loss should allow further understanding whether intervalence band absorption (IVBA) and free carrier absorption are the main controlling mechanisma in the behavior of T_0 and T_1 of semiconductor lasers. From the experiments of our 1.17–1.19 μm InGaAs QW lasers, the measured $T_{\alpha i}$ values ranging from 500 to 1000 K ($d\alpha_i/dT \sim 6 \times 10^{-2}$ cm^{-1}/K) are very high compared to that ($T_{\alpha i}$ = 90–100 K, $d\alpha_i/dT \sim 0.2$ cm^{-1}/K) [3] of the InP-based 1.3-μm lasers. The large $T_{\alpha i}$ of our InGaAs QW lasers, at $\lambda = 1.2$ μm, indicates that IVBA or free carrier absorption are minimal in our lasers, as would be expected for $\lambda = 1.2$ μm.

The material gain parameter, g_o, decreases as a function of increasing temperature [44], [46]. The temperature dependence of the gain parameter, T_{go}, plays a role in the difference between the T_0 values for different cavity length devices as shown in (11). Both the material gain parameters (g_o) of lasers B and C have relatively weak temperature sensitivity, in excess of $T_{go} > 350$ K. T_{go} values for InP-based lasers have not been reported, although they can be estimated from the temperature dependence of the differential gain to be approximately $T_{go} = 200$ K [25]. T_{go} is an important parameter for the investigation of the maximum modulation speed with temperature changes.

VI. Conclusion

We have demonstrated low threshold- and transparency-current density diode lasers and high external quantum efficiency with an emission wavelength of 1.165–1.19 μm, with strain-compensated $In_{0.35}Ga_{0.65}As$ QW and $In_{0.4}Ga_{0.6}As$ QW. Low-threshold-($J_{\rm th}$ = 100 A/cm^2, L = 2000 μm) and low-transparency-current-density ($J_{\rm tr}$ = 59 A/cm^2) strain-compensated $In_{0.4}Ga_{0.6}As$ QW lasers, with an emission wavelength of 1.185-μm, are achieved with high current injection efficiency (η_i = 80%) utilizing AlGaAs as both cladding layers. The increase in current injection efficiency, in laser C, is attributed to the use of p-AlGaAs instead of p-InGaP for the choice of the p-cladding layer, which is consistent with the hypothesis of increased carrier leakage through interfacial defects in lasers A and B.

A simple expansion of T_o [see (11)] and T_1 [see (13)] into the characteristic temperature coefficients for the fundamental device parameters ($T_{\eta i}$, T_{go}, $T_{\rm tr}$, and $T_{\alpha i}$) has been derived. These simple T_0 and T_1 expressions allow practical identification of dominant controlling mechanisms useful for further understanding of the temperature behavior of the semiconductor lasers. The length dependence of T_0 and T_1 are accurately predicted, as confirmed by measurements on InGaAs-active lasers. The studies of the temperature behavior of the physical parameters should allow further insight into optimizing the device design for high T_0 and T_1 values.

Acknowledgment

The authors would like to acknowledge Prof. D. Botez of the University of Wisconsin-Madison, Prof. P. S. Zory, Jr., of the University of Florida-Gainesville, and Prof. P. Blood of the Cardiff University at Cardiff, Wales, for helpful technical discussions on the quantum-well lasers. The authors would also like to acknowledge Dr. R. P. Schneider, Jr., and Dr. D. P. Basile of Agilent Technologies, San Jose, CA, for helpful technical discussion and assistance on the material aspects of the experiments.

References

[1] J. S. Harris, Jr., "Tunable long-wavelength vertical-cavity lasers: The engine of next generation optical networks?," *IEEE J. Select. Topics Quantum Electron.*, vol. 6, pp. 1145–1160, Nov./Dec. 2000.

[2] T. Namegaya, N. Matsumoto, N. Yamanaka, N. Iwai, H. Nakayama, and A. Kasukawa, "Effects of well numbers in 1.3-μm GaInAsP/InP GRIN-SCH strained-layer quantum-well lasers," *IEEE. J. Quantum Electron.*, vol. 30, pp. 578–584, Feb. 1994.

[3] A. F. Phillips, A. F. Sweeney, A. R. Adams, and P. J. A. Thijs, "Temperature dependence of 1.3- and 1.5-μm compressively strained InGaAs(P) MQW semiconductor lasers," *IEEE. J. Select. Topics Quantum Electron.*, vol. 5, pp. 401–412, May/June 1999.

[4] H. C. Casey, Jr., "Temperature dependence of threshold current density on InP–$Ga_{0.28}In_{0.72}As_{0.6}P_{0.4}$ (1.3 μm) double heterostructure lasers," *J. Appl. Phys.*, vol. 56, no. 7, pp. 1959–1964, 1984.

[5] C. Wilmsen, H. Temkin, and L. A. Coldren, *Vertical-Cavity Surface-Emitting Lasers*. Cambridge, U.K.: Cambridge Univ. Press, 1999.

[6] D. I. Babic, K. Streubel, R. P. Mirin, N. M. Margalit, J. E. Bowers, E. L. Hu, D. E. Mars, Y. Long, and K. Carey, "Room-temperature continuous-wave operation of 1.54-μm vertical-cavity lasers," *IEEE Photon. Technol. Lett.*, vol. 7, pp. 1225–1227, Nov. 1995.

[7] J. Boucart, C. Starck, F. Gaborit, A. Plais, N. Bouche, E. Derouin, L. Golstein, C. Fortin, D. Carpentier, P. Salet, F. Brillouet, and J. Jacquet, "1-mW CW-RT monolithic VCSEL at 1.55 μm," *IEEE Photon. Technol. Lett.*, vol. 11, pp. 629–631, June 1999.

[8] E. Hall, S. Nakagawa, G. Almuneau, J. K. Kim, and L. A. Coldren, "Room-temperature, CW operation of lattice-matched long-wavelength VCSELs," *Electron. Lett.*, vol. 36, no. 17, pp. 1465–1467, 2000.

[9] N. Tansu and L. J. Mawst, "High-performance, strain compensated InGaAs–GaAsP–GaAs (λ = 1.17μm) quantum well diode lasers," *IEEE Photon. Technol. Lett.*, vol. 13, pp. 179–181, Mar. 2001.

[10] S. Sato and S. Satoh, "1.21 μm continuous-wave operation of highly strained GaInAs quantum well lasers on GaAs substrates," *Jpn. J. Appl. Phys.*, vol. 38, pp. L990–L992, 1999.

[11] F. Koyama, D. Schlenker, T. Miyamoto, Z. Chen, A. Matsutani, T. Sakaguchi, and K. Iga, "1.2 μm highly strained GaInAs/GaAs quantum well lasers for singlemode fiber datalink," *Electron. Lett.*, vol. 35, no. 13, pp. 1079–1081, 1999.

[12] D. Schlenker, T. Miyamoto, Z. Chen, F. Koyama, and K. Iga, "1.17-μm highly strained GaInAs–GaAs quantum-well laser," *IEEE Photon. Technol. Lett.*, vol. 11, pp. 946–948, Aug. 1999.

[13] W. Choi, P. D. Dapkus, and J. J. Jewell, "1.2-μm GaAsP/InGaAs strain compensated single-quantum well diode laser on GaAs using metal-organic chemical vapor deposition," *IEEE Photon. Technol. Lett.*, vol. 11, pp. 1572–1574, 1999.

[14] M. Kondow, T. Kitatani, S. Nakatsuka, M. C. Larson, K. Nakahara, Y. Yazawa, M. Okai, and K. Uomi, "GaInNAs: A novel material for long wavelength semiconductor lasers," *IEEE J. Select. Topic Quantum Electron.*, vol. 3, pp. 719–730, 1997.

[15] S. Sato and S. Satoh, "Room-temperature continuous-wave operation of 1.24-μm GaInNA's lasers grown by metal-organic chemical vapor deposition," *IEEE J. Select. Topic Quantum Electronics*, vol. 5, pp. 707–710, 1999.

[16] F. Hohnsdorf, J. Koch, S. Leu, W. Stolz, B. Borchert, and M. Druminski, "Reduced threshold current densities of (GaIn)(Nas)/GaAs single quantum well lasers for emission wavelengths in the range 1.28–1.38 μm," *Electron. Lett.*, vol. 35, no. 7, pp. 571–572, 1999.

[17] B. Borchert, A. Y. Egorov, S. Illek, and H. Riechert, "Static and dynamics characteristics of 1.29 μm GaInNA's ridge-waveguide laser diodes," *IEEE Photon. Technol. Lett.*, vol. 12, pp. 597–599, 2000.

[18] M. R. Gokhale, P. V. Studenkov, J. Wei, and S. R. Forrest, "Low-threshold current, high efficiency 1.3-mm wavelength aluminum-free InGaAsN-based quantum-well lasers," *IEEE Photon. Technol. Lett.*, vol. 12, pp. 131–133, 2000.

[19] N. Tansu and L. J. Mawst, "Low-threshold-current strain-compensated InGaAs(N)–GaAsP–InGaP (λ = 1.19–1.3μm) quantum well diode lasers," *IEEE Photon. Technol. Lett.*, vol. 14, pp. 444–446, Apr. 2002.

[20] R. Fehse, S. J. Sweeney, A. R. Adams, E. P. O'Reilly, A. Y. Egorov, H. Riechert, and S. Illek, "Insights into carrier recombination processes in 1.3 mm GaInNAs-based semiconductor lasers attained using high pressure," *Electron. Lett.*, vol. 37, no. 2, pp. 92–93, 2000.

[21] J. Y. Tsao, *Materials Fundamentals of Molecular Beam Epitaxy*. Boston, MA: Academic, 1993, ch. 5, pp. 183–186.

[22] K. Kim and Y. H. Lee, "Temperature-dependent critical thickness for strained-layer heterostructures," *Appl. Phys. Lett.*, vol. 67, no. 15, pp. 2212–2214, 1995.

[23] M. J. Ekenstedt, S. M. Wang, and T. G. Andersson, "Temperature-dependent critical layer thickness for $In_{0.36}Ga_{0.64}As$/GaAs single quantum wells," *Appl. Phys. Lett.*, vol. 58, no. 8, pp. 854–855, 1995.

[24] D. Schlenker, T. Miyamoto, Z. B. Chen, M. Kawaguchi, T. Kondo, E. Gouardes, F. Koyama, and K. Iga, "Critical layer thickness of 1.2-mm highly strained GaInAs/GaAs quantum wells," *J. Cryst. Growth*, vol. 221, pp. 503–508, 2000.

[25] Y. Kwon, W. G. Jeong, Y. Cho, and B. Choe, "Effect of $GaAs_yP_{1-y}$ ($0 < y < 1$) interlayers on the structural, optical, and electrical characteristics of GaAs/InGaP heterojunction," *Appl. Phys. Lett.*, vol. 76, pp. 2379–2381, 2000.

[26] D. Zhou and L. J. Mawst, "Simplified-antiresonant reflecting optical waveguide-type vertical cavity surface emitting lasers," *Appl. Phys. Lett.*, vol. 76, no. 13, pp. 1659–1661, March 2000.

[27] N. Tansu, D. Zhou, and L. J. Mawst, "Low temperature sensitive, compressively-strained InGaAsP active (λ = 0.78–0.85 μm) region diode lasers," *IEEE Photon. Technol. Lett.*, vol. 12, pp. 603–605, June 2000.

[28] T. Miyamoto, private communication, Jan. 2001.

[29] A. Al-Muhanna, L. J. Mawst, D. Botez, D. Z. Garbuzov, R. U. Martinelli, and J. Connolly, "14.3 W quasicontinuous wave front-facet power from broad-waveguide Al-free 970 nm diode lasers," *Appl. Phys. Lett.*, vol. 71, no. 9, pp. 1142–1144, 1997.

[30] D. P. Basile, private communication, Oct. 2001.

[31] L. Shterengas, R. Menna, W. Trussell, D. Donetsky, G. Belenky, J. Connolly, and D. Garbuzov, "Effect of heterobarrier leakage on the performance of high power 1.5 μm InGaAsP multiple-quantum-well lasers," *J. Appl. Phys.*, vol. 88, no. 5, pp. 2211–2214, 2000.

[32] D. Botez and P. Blood, private communication, Jan. 2001.

[33] T. A. DeTemple and C. M. Herzinger, "On the semiconductor laser logarithmic gain–current density relationships," *IEEE. J. Quantum Electron.*, vol. 29, pp. 1246–1252, May 1993.

[34] J. S. Osinski, P. Grodzinski, Y. Zou, and P. D. Dapkus, "Threshold current analysis of compressive strain (0–1.8%) in low-threshold, long-wavelength quantum well lasers," *IEEE J. Quantum Electron.*, vol. 29, pp. 1576–1585, June 1993.

[35] Z. B. Chen, D. Schlenker, F. Koyama, T. Miyamoto, A. Matsutani, and K. Iga, "High temperature characteristics of highly strained 1.2-μm InGaAs/GaAs lasers," in *Proc. APCC/OECC'99*, vol. 2, Beijing, China, 1999, pp. 1311–1314.

[36] T. Kondo, D. Schlenker, T. Miyamoto, Z. B. Chen, M. Kawaguchi, E. Gouardes, F. Koyama, and K. Iga, "Lasing Characteristics of 1.2 μm highly strained GaInAs/GaAs quantum well lasers," *Jpn. J. Appl. Phys.*, vol. 40, no. 1, pp. 467–471, Feb. 2001.

[37] D. P. Bour, D. W. Treat, R. L. Thornton, R. S. Geels, and D. F. Welch, "Drift leakage current in AlGaInP quantum-well lasers," *IEEE. J. Quantum Electron.*, vol. 29, pp. 1337–1343, May 1993.

[38] H. Kressel and J. K. Butler, *Semiconductor Lasers and Heterojunction LEDs*. New York: Academic, 1977, ch. 8, p. 263.

[39] S. R. Chinn, P. S. Zory, Jr., and A. R. Reisinger, "A model for GRIN-SCH-SQW diode lasers," *IEEE J. Quantum Electron.*, vol. 24, pp. 2191–2214, Nov. 1993.

[40] G. Lim, Y. Park, C. A. Zmudzinski, P. S. Zory, Jr., L. M. Miller, T. L. Cockerill, J. J. Coleman, C. S. Hong, and L. Figueroa, "Predicting diode laser performance," *Proc. SPIE*, vol. 1418, pp. 123–131, Jan. 1991.

[41] G. W. Taylor, "Theory of operation of the quantum-well injection laser without k selection," *J. Appl. Phys.*, vol. 70, no. 5, pp. 2508–2535, Sept. 1991.

[42] P. S. Zory, A. R. Reisinger, R. G. Waters, L. J. Mawst, C. A. Zmudzinski, M. A. Emanuel, M. E. Givens, and J. J. Coleman, "Anomalous temperature dependence of threshold for thin quantum well AlGaAs diode lasers," *Appl. Phys. Lett.*, vol. 49, pp. 16–18, 1986.

[43] M. M. Leopold, A. P. Specht, C. A. Zmudzinski, M. E. Givens, and J. J. Coleman, "Temperature-dependent factors contributing to T_o in graded-index separate-confinement-heterostructure single quantum well lasers," *Appl. Phys. Lett.*, vol. 50, pp. 1403–1405, 1987.

[44] L. A. Coldren and S. W. Corzine, *Diode Lasers and Photonics Integrated Circuits*. New York: Wiley, 1995.

[45] G. P. Agrawal and N. K. Dutta, *Semiconductor Lasers*. New York: Van Nostrand, 1993.

[46] Y. Zou, J. S. Osinski, P. Grodzinski, P. D. Dapkus, W. C. Rideout, W. F. Sharfin, J. Schlafer, and F. D. Crawford, "Experimental study of auger recombination, gain, and temperature sensitivity of 1.5 mm compressively strained semiconductor lasers," *IEEE J. Quantum Electron.*, vol. 29, pp. 1565–1575, June 1993.

[47] S. L. Chuang, *Physics of Optoelectronic Devices*. New York: Wiley, 1995.

[48] K. J. Vahala and C. E. Zah, "Effect of doping on the optical gain and spontaneous noise enhancement factor in quantum well amplifiers and lasers studied by simple analytic expressions," *Appl. Phys. Lett.*, vol. 52, pp. 1945–1947, 1988.

[49] W. W. Lui, T. Yamanaka, Y. Yoshikuni, S. Seki, and K. Yokoyama, "Temperature Sensitivity of Auger-recombination effects in compressively strained InGaAs/InGaAsP quantum well lasers," *Phys. Rev. B*, vol. 48, pp. 8814–8822, 1993.

[50] Z. M. Li and T. Bradford, "A comparative study of temperature sensitivity of InGaAsP and AlGaAs MQW lasers using numerical simulations," *IEEE J. Quantum Electron.*, vol. 31, pp. 1841–1847, Oct. 1995.

[51] A. Ghiti, M. Silver, and E. P. O'Reilly, "Low threshold current and high differential gain in ideal tensile- and compressive-strained quantum well lasers," *J. Appl. Phys.*, vol. 71, no. 9, pp. 4626–4628, 1992.

[52] T. Higashi, T. Yamamoto, S. Ogita, and M. Kobayashi, "Experimental analysis of characteristic temperature in quantum-well semiconductor lasers," *IEEE J. Select. Topic Quantum Electron.*, vol. 3, pp. 513–521, 1997.

[53] P. Abraham, J. Piprek, S. P. DenBaars, and J. E. Bowers, "Improvement of internal quantum efficiency in 1.55 mm laser diodes with InGaP electron stopper layer," *Jpn. J. Appl. Phys.*, vol. 38, pt. 1, no. 2B, pp. 1239–1242, Feb. 1999.

[54] R. F. Nabiev, E. C. Vail, and C. J. Chang-Hasnain, "Temperature dependent efficiency and modulation characteristics of Al-free 980-nm laser diodes," *IEEE J. Select. Topic Quantum Electron.*, vol. 1, pp. 234–243, 1995.

[55] L. J. Mawst, A. Bhattacharya, M. Nesnidal, J. Lopez, D. Botez, J. A. Morris, and P. S. Zory, Jr., "High continuous wave output power InGaAs/InGaAsP/InGaP diode lasers: Effect of substrate misorientation," *Appl. Phys. Lett.*, vol. 67, no. 20, pp. 2901–2903, Nov. 1995.

[56] P. M. Smowton and P. Blood, "The differential efficiency of quantum-well lasers," *IEEE J. Select. Topic Quantum Electron.*, vol. 3, pp. 491–498, 1997.

[57] P. A. Andrekson, N. A. Olsson, T. Tanbun-Ek, R. A. Logan, D. Coblentz, and H. Temkin, "Novel technique for determining internal loss of individual semiconductor lasers," *Electron. Lett.*, vol. 28, pp. 171–172, 1992.

[58] P. Blood, private communication, Nov. 2001.

[59] D. A. Ackerman, P. A. Morton, G. E. Shtengel, M. S. Hybertsen, R. F. Kazarinov, T. Tanbun-Ek, and R. A. Logan, "Analysis of T_o in 1.3 μm multi-quantum-well and bulk active lasers," *Appl. Phys. Lett.*, vol. 66, no. 20, pp. 2613–2615, 1995.

[60] N. Tansu and L. J. Mawst, "Temperature sensitivity of InGaAs(N) (λ = 1.19-1.31 μm) quantum well diode lasers," *IEEE Photon. Technol. Lett.*, to be published.

Nelson Tansu was born in Medan, North Sumatra, Indonesia, in 1977. He received the B.S. degree (*summa cum laude*) in applied mathematics, electrical engineering, and physics in 1998 from the University of Wisconsin-Madison, where he is currently working toward the Ph.D. degree in the Department of Electrical and Computer Engineering.

He is a recipient of the Bohn Scholarship, the WARF graduate fellowship, and the Vilas graduate fellowship. His research includes design, fabrication, and MOCVD growth of novel-active-material GaAs-based vertical-cavity surface-emitting lasers (VCSELs) for all practical transmission window of optical-communications systems, 850-mm VCSELs (InGaAsP QW), 1300-nn VCSELs (InGaAsN QW), and 1550-nm VCSELs. His focus is also on the physics of semiconductor QW lasers encompassing recombination mechanisms, optical gain, carrier transport, and temperature characteristics. His other research interests include tunable lasers, semiconductor optical amplifiers and modulators, and nonlinear optics in semiconductors.

Ying-Lan Chang received the B.A. degree in electrical engineering from National Tsing-Hua University, Taiwan, R.O.C., the M.S. degree in electrical engineering from Princeton University, Princeton, NJ, and the Ph.D. degree in materials from the University of California at Santa Barbara.

She was with Hewlett Packard Laboratories, Palo Alto, CA, where she contributed to the development of TS AlGaInP and GaN light-emitting diodes. Since joining Agilent Laboratories, Palo Alto, CA, in 2000, she has been actively involved in the research and development of long-wavelength VCSELs. She has authored or co-authored 40 journal articles and over 50 conference presentations and is named as co-inventor on a number of patents.

Tetsuya Takeuchi received the B.A. and M.S. degrees in electrical engineering from Nagoya University, Japan, in 1990 and 1992, respectively, and the Ph.D. degree in electrical engineering from Meijo University, Japan, in 1999.

After joining HP/Agilent Laboratories, Palo Alto, CA, he has been working on the III–V semiconductor material growth and characterizations. He was engaged in the MBE growth of InGaAs laser diodes and also the MOCVD growth of GaN-based UV laser diodes and blue/green light-emitting diodes. He recently has developed the MOCVD growth process of InGaAsN long-wavelength vertical-cavity surface-emitting lasers.

David P. Bour (F'00) received the B.S. degree in physics from Massachusetts Institute of Technology (MIT), Cambridge, in 1983 and the Ph.D. degree in electrical engineering from Cornell University, Ithaca, NY, in 1987.

From 1987 to 1991, he was a Member of Technical Staff at Sarnoff Corporation, Princeton, NJ. From 1991 to 1999, he was a Principal Scientist in the Electronic Materials Laboratory, Xerox Palo Alto Research Center, Palo Alto, CA, fabricating nitride blue laser diodes and phosphide red laser diodes for laser printing. He is currently a Department Scientist in the Communications and Optics Research Laboratory at Agilent Laboratories, Palo Alto, CA, where he is working on the epitaxial growth of semiconductor lasers by metalorganic chemical vapor deposition.

Scott W. Corzine was born in Nashville, TN, in 1963. He received the B.S., M.S., and Ph.D. degrees in electrical engineering from the University of California at Santa Barbara. His graduate work involved the theoretical and experimental investigation of vertical-cavity surface-emitting lasers.

He is currently with Agilent Laboratories, Alto, CA, working on the design and fabrication of various optoelectronic devices. He is co-author of a graduate-level textbook on semiconductor lasers and has also contributed a chapter to a book on QW lasers.

Michael R. T. Tan was born in Manila, The Philippines, in 1954. He received the B.Sc. degree in electrical engineering from California State University at Long Beach in 1976 and the M.S. and Ph.D degrees in electrical engineering from Stanford University, Stanford, CA, in 1978 and 1982, respectively.

He joined Hewlett Packard Laboratories (now Agilent Laboratories), Alto, CA, in 1984 as a Member of Technical Staff, where he was engaged in the development of advanced surface acoustic wave filters, traveling-wave electrooptic modulators, nonlinear transmission lines, and other millimeter-wave devices. His research led to the development of several HP instruments, including the HP71500A Microwave transition analyzer and the HP54124 50-GHz sampling oscilloscope. From 1991 to 1998, his research was focused on the development of 980- and 850-nm vertical-cavity surface-emitting lasers (VCSELs) for data communications, which led to the development of HP's first 850-nm VCSEL-based multimode transceiver product in 1997. During the same period, he worked on single-mode 780-nm VCSEL arrays for printing application, 850-nm and 980-nm VCSEL arrays for parallel optic short-reach applications and on 650-nm VCSELs for plastic optical-fiber application. His current research interest is focused on the development of long-wavelength VCSELs.

Luke J. Mawst (M'88–SM'93) was born in Chicago, IL, in 1959. He received the B.S. degree in engineering physics and the M.S. and Ph.D. degrees in electrical engineering from the University of Illinois at Urbana-Champaign in 1982, 1984, and 1987, respectively. His dissertation research involved the development of index-guided semiconductor lasers and laser arrays grown by MOCVD.

He joined TRW, Inc., Redondo Beach, CA, in 1987, where he was a Senior Scientist in the Research Center, engaged in the design and development of semiconductor lasers using MOCVD crystal growth. He is co-inventor of the Resonant Optical Waveguide (ROW) antiguided array and has contributed to its development as a practical source of high coherent power. He developed a novel single-laser structure—the ARROW laser—as a source for coupling high powers into fibers. He has also been involved in the development of 2-D coherent surface-emitting arrays, vertical-cavity surface emitters (VCSELs), and distributed-feedback laser structures. He is currently an Associate Professor at the University of Wisconsin-Madison, where he is involved in the development novel III/V compound semiconductor device structures, including (VCSELs), active photonic lattice structures, and high-power Al-free diode lasers. He has authored or co-authored more than 100 technical papers and holds 13 patents.

Dr. Mawst received the TRW Group Level Chairman's Award for his work on the ROW antiguided array.